Published in final edited form as:
J Phys Chem B. 2013 October 3; 117(39): 11719–11731. doi:10.1021/jp405862p.

Liquid-Vapor Interfacial Properties of Aqueous Solutions of Guanidinium and Methyl Guanidinium Chloride: Influence of Molecular Orientation on Interface Fluctuations

Shuching Ou, **Di Cui**, and **Sandeep Patel***
Department of Chemistry and Biochemistry, University of Delaware, Newark, Delaware 19716, USA

Abstract

The guanidinium cation (C(NH2)3+) is a highly stable cation in aqueous solution due to its efficient solvation by water molecules and resonance stabilization of the charge. Its salts increase the solubility of nonpolar molecules (”salting-in”) and decrease the ordering of water. It is one of the strongest denaturants used in biophysical studies of protein folding. We investigate the behavior of guanidinium and its derivative, methyl guanidinium (an amino acid analogue) at the air-water surface, using atomistic molecular dynamics (MD) simulations and calculation of potentials of mean force. Methyl guanidinium cation is less excluded from the air-water surface than guanidinium cation, but both cations show orientational dependence of surface affinity. Parallel orientations of the guanidinium ring (relative to the Gibbs dividing surface) show pronounced free energy minima in the interfacial region, while ring orientations perpendicular to the GDS exhibit no discernible surface stability. Calculations of surface fluctuations demonstrate that near the air-water surface, the parallel-oriented cations generate significantly greater interfacial fluctuations compared to other orientations, which induces more long-ranged perturbations and solvent density redistribution. Our results suggest a strong correlation with induced interfacial fluctuations and ion surface stability. These results have implications for interpreting molecular-level, mechanistic action of this osmolyte’s interaction with hydrophobic interfaces as they impact protein denaturation (solubilization).

Keywords

molecular dynamics; guanidinium; interface; fluctuations

I. INTRODUCTION

The search for unifying and predictive theoretical foundations for describing a broad spectrum of specific-ion effects continues to garner significant scientific attention. Specific-ion effects are relevant to a vast spectrum of biological and physical processes. These range

*Corresponding author. sapatel@udel.edu.

Supporting Information Available Supporting Information discusses aspects of simulation protocol, analysis of bulk structural properties of solutions, Kirkwood-Buff analysis, discussion of uncertainty calculations, and analysis of bulk pair distribution functions of Gdm^+ and M-Gdm^+ solutions. This information is available free of charge via the Internet at http://pubs.acs.org.

from the differential stabilities of proteins in solution mediated by different ions, to interfacial propensities of inorganic halide ions to various interfaces, to modulation of aggregation kinetics of nanomaterials[1–18]. The effects are distributed across mono-valent (simple) to molecular ions as well. As such, the need for a unifying picture is clear. One particular specific-ion effect involves the effects of osmolytes and co-solvents in modulating the stability of folded versus unfolded states of proteins[19–21]. In particular, guanidinium chloride (as well as urea) is a well-known protein chemical denaturant[19–22]. Investigations into the mechanism of guanidinium's (Gdm^+) influence on protein stability have enjoyed a long history, though questions of mechanism still remain[23].

Focusing on a series of molecular simulations studies of interaction of guanidinium with hydrophobic systems, we draw attention to the very specific orientation adopted by the osmolyte when interacting with the model solutes in these studies[24]; this study demonstrates that guanidinium moieties orient in a parallel manner in the region next to hydrophobic surfaces. This has implications for the association of guanidinium with hydrophobic and planar, pi-electron rich sidechains of proteins. Intriguingly, the orientation of the guanidinium is parallel to the hydrophobic surface, vis-a-vis, the protein sidechain-solution interface. This orientation has been rationalized as arising from its ability to optimize the overall hydration properties of the complex (i.e. peptide-guanidinium). Though controversies about the interaction of guanidinium with backbone moieties or sidechains, dispersion versus electrostatic interactions driving these associations, have abounded in the literature, the structural association with guanidinium (at least from a simulation perspective) appears quite general. Since the influence of co-solvents or osmolytes must occur through/at an interface, we consider investigations of interfacial properties involving these chemical components a relevant area of focus. Furthermore, since hydrophobic moieties are often implicated in discussions of the association of the guanidinium cation with peptide or peptide-like solutes, we here consider a much simpler interface, the aqueous liquid-vapor (L-V) interface, as a proxy to a chemically defined hydrophobic interface. A fundamental question we seek to address concerns the relationship of the orientation of the guanidinium cation to its influence on interfacial properties in the context of how this effect mediates the observed nature of association of guanidinium with a molecular surface/interface. Recent studies[25,26] have begun to uncover the relation between interfacial stability of ionic species (such as spherical monovalent ions) and induced interfacial fluctuations (specifically at model liquid-vapor interfaces). These studies indicate that species with interfacial stability tend on average to induce higher interfacial fluctuations. Moreover, the differing propensities of various ions to induce varying degrees of interfacial fluctuations is shown to be related to the local solvation environment of the ion and how this local environment couples to solvent further away from the ion. It is this coupling that is critical in the facilitating fluctuations. This leads to the question of whether this effect can be observed for the guanidinium species already mentioned, and further, if this effect depends on the orientation of the molecule relative to the interface. A novel aspect of the following study is the analysis of induced interfacial fluctuations and their orientational dependence.

We consider several aspects related to aqueous solution liquid-vapor interfaces of guanidinium,Gdm^+, and methyl guanidinium, M-Gdm^+ (an amino acid analogue), interfaces of varying concentrations. We consider structural and thermodynamic aspects as considered

in earlier studies using varying force fields, aiming to draw comparisons and contrasts in current modeling approaches to these systems. We further characterize the thermodynamics of the interface by computing potentials of mean force describing system free energetics as it depends on the location of a single Gdm^+/M-Gdm^+ (infinite dilution limit) from the liquid-vapor interface. Computational experiments measuring the reversible work (potential of mean force, PMF) for transferring single ions/molecules from bulk aqueous environment to the aqueous solution liquid-vapor interface have enjoyed a long history as a means to explore the origins of surface stability[27–29]. To this end, we also anticipate insights into the details of interfacial stability (or lack of) based on PMF calculations. We further probe the influence of the molecular ions on interfacial fluctuations, again restricting our attention to the infinite dilution limit of a single ion in solution. It has been shown for the case of spherically symmetric ions that the magnitude of aqueous interfacial fluctuations is intimately related to the nature of the solute species[25,26], its interfacial stability, and hydration. In this study, we examine the interconnections between surface stability, hydration, and orientation of molecular ions as they impact on interfacial fluctuations and how these may be of relevance to a variety of osmolyte-mediated protein stability effects in biomacromolecular systems.

This study is organized as follows. In Section II we discuss the force fields and computational details. Our results are presented in Section III and are organized into three topics. We start with examining the density profiles of solutes and solvent, surface tension under different concentrations, and surface excess of ionic species in Section IIIA. In Section III B we consider free energetics for single Gdm^+/M-Gdm^+ through the liquid-vapor interface. We further investigate the interfacial fluctuations of the aqueous interface in Section IIIC. We conclude our study in Section IV with a summary of our findings and general discussion.

II. METHODS

Molecular dynamics simulations were performed using the CHARMM package[30]. Simulations of liquid-vapor interfaces were performed in the *NVT* ensemble. Temperature was maintained at $T = 300$ K using Nosé-Hoover thermostat[31] with a thermal piston mass of 50 kcal/mol · ps^2. The system contained 38, 71, 107, 142 or 190 pairs of guanidinium (or methyl guanidinium) and chloride ions, with 1977 water molecules (represented by the polarizable TIP4P-FQ model[32]) per unit cell, which resulted in molal concentration of 1.1, 2, 3, 4, 5.3 m, respectively. The simulation cell was rectangular with dimensions 40 Å × 40 Å × 150 Å, in which z is the direction normal to the liquid-vapor interface. Long-range electrostatics were accounted for by Particle mesh Ewald (PME) summation[33,34] with a 40 × 40 × 150 $Å^3$ Fast Fourier transform (FFT) grid, sixth order B-spline interpolation, and screening parameter $\kappa = 0.33$. Dynamics were propagated using the Leapfrog Verlet integrator[35] with a 0.5 fs time step. The actual position of Gibbs Dividing Surface (GDS) at corresponding concentration, which is determined by half of bulk water oxygen density, is summarized in Table I. Four different replicates were used and the first 1 ns of each replicate was considered as equilibration. At least 15 ns of production run for each replicate was used to compute properties such as density profiles and surface tensions.

Moreover, in order to illustrate the molecular detail and free energetics of Gdm^+/M-Gdm^+ with the presence of L-V interfaces, we simulated a system with 1977 TIP4P-FQ water molecules and single Gdm^+/M-Gdm^+, with the corresponding GDS around ± 18 Å from the center of water box. For potential of mean force calculations, our reaction coordinate, ξ_0, is the Cartesian *z*-component of the separation between the water slab center of mass and Gdm^+/M-Gdm^+ center of mass; with this collective variable definition, no corrections for Jacobian or Leibniz transformations are required (See Supporting Information and Reference[36]). In all simulations used for computing potentials of mean force, Gdm^+/M-Gdm^+ were restrained to *z*-positions from 0 Å to 30 Å relative to the water slab center of mass using a harmonic potential $\mathrm{U}_{restraint}(z;z_{relative,ref})=\frac{1}{2}k_{restraint}(z-z_{relative,ref})^2$ with the force constant of 4 (kcal/mol)/Å^2; this encompasses a range approximately 18 Å below the GDS to approximately 12 Å above it at 300 K. Again, the first 1 ns for each restraining window was considered as equilibration; the following 20 ns of data for each umbrella sampling window was used to compute the properties of single Gdm^+/M-Gdm^+. The PMF is computed using WHAM[37] and is defined to be zero in the bulk (which is determined by the window z = 0 Å), as presented in Figure 3a. The uncertainties in potentials of mean force are determined using the approach of Zhu and Hummer[38]:

$$\mathrm{var}[G(\xi_{\mathrm{N}})] \approx \sum_{i=1}^{N} \mathrm{var}[K\Delta\xi\bar{z}_i] \quad (1)$$

where $z_{\mathrm{i}}\bar{}$ is the mean position of z in the i_{th} window, which can be obtained from block averages[39]. The corresponding standard deviation $\sigma[G(\xi_{\mathrm{N}})]$ is then the square root of $\mathrm{var}[G(\xi_{\mathrm{N}})]$. In our case, $G(z = 0\ \text{Å}) = 0$, therefore the window z = 30 Å is expected to have the largest uncertainty. The largest uncertainties for the systems are approximately 0.1 kcal/mol (shown in Supporting Information, Figure 9).

The polarizable TIP4P-FQ water model employs a rigid geometry having an O-H bond distance of 0.9572 Å, an H-O-H bond angle of 104.52° and a massless, off-atom *M* site located 0.15 Å along the H-O-H bisector which carries the oxygen partial charge. The non-bond interactions were treated via the standard Lennard-Jones "12-6" potential

$$E_{LJ}=\sum_{ij}\varepsilon_{ij}\left(\frac{R_{\mathrm{min},ij}^{12}}{r_{ij}^{12}}-2\frac{R_{\mathrm{min},ij}^{6}}{r_{ij}^{6}}\right) \quad (2)$$

Lennard-Jones interactions were gradually switched off at interparticle distance of 12 Å, with a gradual switching between 11 Å and 12 Å using the switching function:

$$S(r_{ij})=\begin{cases} 1 & r_{ij}\le r_{\mathrm{on}} \\ \frac{(r_{\mathrm{off}}^2-r_{ij}^2)^2(r_{\mathrm{off}}^2+2r_{ij}^2-3r_{\mathrm{on}}^2)}{(r_{\mathrm{off}}^2-r_{\mathrm{on}}^2)^3} & r_{\mathrm{on}}<r_{ij}\le r_{\mathrm{off}} \\ 0 & r_{ij}>r_{\mathrm{off}} \end{cases} \quad (3)$$

Repulsion and dispersion interactions are modeled using a single Lennard-Jones (LJ) site located on the oxygen center having parameters $R_{\mathrm{min,O}}$ = 3.5459 Å and ε_{O} = 0.2862 kcal mol^{-1}.

The charge equilibration (CHEQ) polarizable force field model for guanidinium and methyl guanidinium (M-Gdm^+) cations was constructed by adapting the CHARMM CHEQ force field for proteins,[40,41] extending the electrostatic parameters, hardnesses and electronegativities from the protein force field for an arginine side chain. For details of the CHEQ formalism and the application of this force field for methyl guanidinium, please refer to supporting information or Reference[42]. In the present work, the methyl guanidinium was partitioned into two charge normalization units (charge conserved with this unit) to control polarizability scaling[42]. The first unit encompasses the methyl (-CH_3) and secondary amine (-NH) groups while the second unit includes the central carbon and two primary amine groups (-$C(NH_2)_2$). For the force field of guanidinium cation (Gdm^+) we use the same analogue with M-Gdm^+ by replacing the methyl and secondary amine groups with another -NH_2 group, consider the whole cation as one unit. This partitioning allows for consistency with the existing CHARMM CHEQ protein force field and permits use of the existing non-bond (LJ and electrostatic) parameters for arginine from the polarizable force field[40,41]. The force field parameters for guanidinium chloride and methyl guanidinium chloride are summarized in Table III. In Reference[42], validation of the present force field was presented in terms of interactions of the guanidinium group with water relative to predictions from ab initio calculations at the MP2 correlated level, as well as hydration free energies of methyl guanidinium compared with previous simulation and experimental estimate data. Furthermore, as will be apparent from the discussion of results below, the predictions of the present force field show rather strong consistency with previous force fields studying similar systems[43]. Finally, in the SI, we show results of Kirkwood-Buff analysis for the 1.1 m systems (as was done in Reference[43]). Though the current force field overestimates activity derivatives, while capturing the concentration dependence, we feel that the current combination of water and cation force field is sufficiently robust considering the range of validation metrics for use in addressing the questions posed.

The non-bond interactions between M-Gdm^+ and solvent species (water and chloride), were validated through the comparison of gas-phase small molecule geometries and interaction energies calculated using the CHEQ force field with those calculated using MP2/aug-cc-pVTZ level quantum mechanics[42]. In the absence of laborious reparameterization of the methyl guanidinium interactions with all system species, we consider it sufficient that for the purposes of the present work, the trend of relative interaction strengths based on QM and force field calculations are equivalent. The further validation with Kirkwood-Buff analyses for Gdm^+/M-Gdm^+ is presented in the Supporting Information (Figures 3 and 4). Cl^- is treated as a non-polarizable Lennard-Jones sphere. The force field combination with water has been validated via calculation of single ion hydration free energies of both ions using accepted free energy methods in conjunction with appropriate corrections for condensed-phase simulation artifacts[44–46].

Charge degrees of freedom for the TIP4P-FQ water molecules and $Gdm^+/M-Gdm^+$ were coupled to a thermostat at 1K using the Nosé-Hoover method[31,47]. Charge degrees of freedom were assigned fictitious masses of 0.000069 and 0.000099 kcal mol^{-1} ps^2 e^{-2}. The charge degrees of freedom were propagated in an extended Lagrangian formalism[32]. Each water molecule was taken as a charge normalization unit. No charge transfers between water

molecules or between water and Gdm^+/M-Gdm^+. We acknowledge recent developments of charge transfer models of water[48,49], and anticipate that application of charge transfer models to the study of condensed phase system with further underlying physics will provide further novel insights.

III. RESULTS

We first consider system properties related to the interface as presented in earlier studies as a means to consider similarities in behavior using different force fields. These properties include density profiles of system components along the dimension normal to the interface, surface tension, and orientations of the guanidinium salts at the interface. We then connect aspects of the orientational structure to thermodynamics at the interface; in order to accomplish this, we also provide a discussion of the estimated PMF's.

A. Density Profile and Surface Tension of Solution

For the osmolyte solutions, we considered number density profiles of the center carbon of Gdm^+/M-Gdm^+, Cl^- and water oxygen along the *z*-dimension, normal to the L-V interface, as shown in Figure 1. The profiles are calculated by averaging over two equivalent halves of the slab, normalized by the density values at the center of the slab; the GDS is taken to be the zero and negative x-axis values indicate movement into the bulk solution and positive values movement towards the vacuum. The position of GDS is determined by the *z*-position where the water density is one-half of the bulk value for the corresponding system, as listed in Table I. Solid curves represent data for the M-Gdm^+ system, dashed curves for the Gdm^+. Statistical uncertainties are less than 0.3% determined from the variance of 4 independent replicates (absolute values of standard deviation are shown in Figure 5 of the Supporting Information). The water oxygen density profiles show little change as a function of cation concentration; in the case of Gdm^+, there is a slight shift of the GDS to larger value, correlating with the expansion of the Gdm^+ density at higher concentration (Figure 1a, b). Furthermore, a density fluctuation feature emerges in the 5.3m Gdm^+ system; this is explained by the higher Gdm^+ density at higher concentrations. Figure 1c and d show variation of M-Gdm^+ and Gdm^+ at 1.1m and 5.3m concentrations, respectively. At low concentrations, 1.1m, we observe no apparent interfacial enhancement of either cation. For the 1.1m systems, due to its hydrophobic methyl group, the M-Gdm^+ solution populates configurations where the cation is closer to the GDS. The Gdm^+, relative to the M-Gdm^+ is substantially more depleted in the region of and just below the GDS, with an associated elevated density in the next layer towards the bulk. At the higher 5.3m concentration, electrostatic interactions between charged cations lead to higher Gdm^+ density in the region of the GDS. the M-Gdm^+ density profile shows an oscillatory behavior, with enhancement relative to the bulk value below the GDS. Thus, in both systems, we observe increased population of the interfacial region by both cations, with the more hydrophobic M-Gdm^+ consistently showing greater propensity for the interface. The Cl^- anion in both solutions at both concentrations correlates with the density profiles of the cations. In contrast to the density profiles shown in Reference[43], we do not observe a shoulder (representing orientations of the guanidinium ring that are parallel to the interface) in the Gdm^+ density profile below the GDS. This suggests that if multiple orientations are viable at the interface

under the force fields we use, then there may be little difference in relative stabilities of the parallel and perpendicular orientations relative to the bulk. We will turn to free energetics of the two orientations further below. We stress that the lack of a shoulder in the present Gdm^+ density profiles (in contrast to those in Reference[43]) does not suggest the absence of a difference in stabilities (relative probabilities) of the two orientations, merely a difference in the degree of stability of one or both relative to the state where the cation is in the bulk. We will address the free energy related to orientations in Section IIIB.

The surface tension of a liquid arises from the imbalance of intermolecular forces at the surface of a L-V interface. We calculate the surface tension for the liquid-vapor interface at each concentration from the average difference in the normal and tangential elements of the internal pressure tensor[50], which is

$$\gamma=\frac{L_z}{2}(P_{zz}-\frac{P_{xx}+P_{yy}}{2}) \quad (4)$$

where P_{xx}, P_{yy}, and P_{zz} are the diagonal elements of the internal pressure tensor and L_z is the length of the simulation cell in the direction normal to the surface. Figure 2 shows surface tension variation with molal concentration for the two salt solutions. As measured experimentally, the Gdm^+ salt solution shows increasing surface tension[23]. However, the experimental surface tension versus concentration slope is not as large as estimated with the current force field combination. The current force field overestimates measured values given in Reference[23].

Nevertheless, both the current simulations and experiment consistently indicate a net surface depletion of the cation as often associated with surface tension increases of aqueous solutions of mono-valent inorganic ions[51]. The M-Gdm^+ surface tension is systematically lower as one would expect due to the slightly higher interfacial propensity of the methyl analogue as reflected in density profiles. In molecular simulations, the surface excess is easier to converge than the surface tension. The surface excess of a solute is considered as[51]

$$\Gamma_s=-\frac{1}{RT}\left(\frac{\partial\gamma}{\partial\ln a_s}\right)_T \quad (5)$$

where R is the gas constant, T is the temperature, γ is the surface tension, and a_s is the activity of the solute. In general, for the case of salt solution, a_s is expressed as $a_s = (f^{\pm} \times m)^{\upsilon}$, where $f^{\pm}$ is the mean activity coefficient of the two dissociated ions, m is the molal concentration, and υ is the sum of the stoichiometric coefficients ($\upsilon = 2$ in this case). We can therefore extract a_s and γ from experiments (refer to Ref[23]) and compute Γ_s at the corresponding concentration by polynomial fitting of γ as a function of $\ln a_s$, as shown in the Supporting Information (Figure 13). The results of Γ_s are shown in Table II.

For our simulation data, we compute the surface excess of a solute with respect of the solvent as[2,51]

$$\Gamma_s = \int_{-\infty}^{z_{\mathrm{Gibbs}}} [\rho_s(z) - \rho_{sb}] dz + \int_{z_{\mathrm{Gibbs}}}^{\infty} \rho_s(z) dz \quad (6)$$

where $\rho_s(z)$ is the density profile of the solute and ρ_{sb} is the bulk density of the corresponding solute. We summarize our results from simulations in Table II as well. The values of the individual ions as well as the total solute (which turns out to be the sum of the individual ion surface excesses) follow qualitatively the experimental trend as a function of guanidinium chloride concentration. As observed for other polarizable force fields used for monovalent inorganic ions[51], the present force field combination overestimates surface excesses.

B. Free Energetics and Orientational Preference

Next we consider the potential of mean force of single Gdm^+/M-Gdm^+ through L-V interface. No minimum is found for both cations with M-Gdm^+ being slightly more stable than Gdm^+. The planar geometry of both cations lends itself to an analysis of the free energetics associated with its unique orientations relative to the interface normal. Here we use the same convention from Reference[43] to define the orientation of the cations (the planar ring of each cation) relative to the L-V interface: the angle θ between the normal vector of the Gdm^+/M-Gdm^+ plane and the *z*-axis. θ ranges from 0 to 90°, when θ = 0°, the Gdm^+/M-Gdm^+ cation is parallel to the L-V interface. The Gdm^+/M-Gdm^+ normal is computed from the cross product of two of the three carbon-nitrogen vectors (in the case of M-Gdm^+, the nitrogens on -NH_2 groups are chosen). We can then select the configurations with the angular conditions for each PMF window to construct the conditional potential of mean force $w(z, \theta)$ by using WHAM. We categorize the orientations with the condition $\theta_0 - \frac{\Delta\theta}{2} \leq \theta \leq \theta_0 + \frac{\Delta\theta}{2}$, with θ_0 = 0, 30, 60, 90°, Δθ = 10°. To assess the reliability of the PMF's we show the overlap distributions between umbrella windows in the Supporting Information (Figure 10); to address convergence, we claim that since the PMF's computed in an unambiguously different way than the angular probability distributions discussed in the next section provide the same information (i.e. that the stability of unique orientations, or their probabilities, are higher at the interfacial region) the PMF's are converged at least for qualitative discussion.

The result of the conditional PMF for Gdm^+/M-Gdm^+ cation is shown in Figure 3b and c, respectively. When θ = 0°, both cations show minima of roughly 0.5 kcal/mol, indicating preferred parallel configurations in the vicinity of the interface; this is consistent with the probability distributions of orientations as will be discussed further below. As θ increases, the corresponding conditional PMF becomes more repulsive; interestingly, M-Gdm^+ still behaves less repulsive than Gdm^+ at the same conditional θ_0.

Following Wernersson et al[43], to quantify the orientational profile of the Gdm^+/M-Gdm^+ in a statistical manner, we consider the (coarse-grained) probability of the single solute at position z' with orientation θ as

$$P(z',\theta)=\frac{\int_{z'-\frac{\Delta z}{2}}^{z'+\frac{\Delta z}{2}}dz\int_{cos(\theta_0-\frac{\Delta\theta}{2})}^{cos(\theta_0+\frac{\Delta\theta}{2})}dcos\theta n(r,z',\theta)}{\int_{z'-\frac{\Delta z}{2}}^{z'+\frac{\Delta z}{2}}dz\int_{-1}^{1}dcos\theta n(r,z',\theta)} \quad (7)$$

where $r=\sqrt{x^2+y^2}$ is the radial distance from the center carbon atom of Gdm^+/M-Gdm^+ in the plane of the surface. $n(r, z', \theta)$ denotes the number count of Gdm^+/M-Gdm^+ with the properties at (z', θ). For each bin region $(z'-\frac{\Delta z}{2}, z'+\frac{\Delta z}{2})$, we have $\int_{-1}^{1}dcos\theta P(z',\theta)=1$. The results of $P(z', \theta)$ for single Gdm^+/M-Gdm^+ are given in Figure 4a and b. Again as a reminder, when $|cos(\theta)| = 1$, the ion is parallel to the L-V interface; the ion is perpendicular to the interface when $|cos(\theta)| = 0$. We further calculate the second order Legendre polynomial using

$$\langle P_2(cos\theta)\rangle=\frac{1}{2}\langle(3cos^2\theta-1)\rangle \quad (8)$$

to measure the degree of orientation of the cations relative to the interface normal. When the orientational configurations are completely random and isotropic, P_2 is zero, whereas for the perfectly aligned case $\langle P_2(cos\theta)\rangle = 1$. $\langle P_2(cos\theta)\rangle = -0.5$ when the orientations are entirely perpendicular. This parameter is then a measure of the uniaxial behavior of the species. The results for θ are shown in Figure 4c, when the restrained position is above $z = 15$ Å, $\langle P_2(cos\theta)\rangle$ for both cations start to increase, indicating enhanced alignment of the cations.

Both cations show no orientational preference when they are in the bulk ($z \leq 13$, which is 5 Å below the GDS); as the ion approaches the GDS, both Gdm^+ and M-Gdm^+ show enhanced probability of configurations parallel to the L-V interface. This orientational preference of Gdm^+ is consistent with the previous studies by Mason et al[20], Koishi et al[24] and Wernersson et al[43] using nonpolarizable force fields. They explained this preference with the weak and anisotropic hydration of Gdm^+ cation. Unlike with spherical cations, the hydration of Gdm^+ is limited to very few water molecules capable of forming hydrogen bonds within the planar surface of Gdm^+. Therefore, in the parallel orientation, desolvation occurs more facilely as the ion nears the L-V interface. This can be connected to the efficiency of guanidinium cation as a denaturant via interactions with the hydrophobic side chains of proteins. Recently, new insights of the surface fluctuations to explain the anionic surface stability have been proposed based on the capillary wave theory[25,26,52]. We will continue this discussion in the next section.

From Figure 4a and b we also observe that Gdm^+ shows stronger parallel preference near the L-V interface (as displayed with higher probability). As the cations move toward the vapor phase, the distribution profile of Gdm^+ recovers to equal for all orientations and bulk-like; on the other hand, M-Gdm^+ shows depletion of parallel configurations and increases the probability of being perpendicular to the L-V interface. We explain this by examining the second order Legendre polynomial of the cations. Define the angle β between positive *z*-axis and the vector constructed from center carbon to the nitrogen of -$NH(CH_3)$ $(\overrightarrow{CN_M})$ for M-

Gdm^+, we then compute the coarse-grained probability of the M-Gdm^+ at position z' with angle β as

$$P(z',\beta)=\frac{\int_{z'-\frac{\Delta z}{2}}^{z'+\frac{\Delta z}{2}}dz\int_{cos(\beta_0-\frac{\Delta\beta}{2})}^{cos(\beta_0+\frac{\Delta\beta}{2})}dcos\beta n(r,z',\beta)}{\int_{z'-\frac{\Delta z}{2}}^{z'+\frac{\Delta z}{2}}dz\int_{-1}^{1}dcos\beta n(r,z',\beta)} \quad (9)$$

The results are shown in Figure 4d. As the M-Gdm^+ crosses through the L-V interface, *cos*β becomes more positive, which implies larger probability of C-$NH(CH_3)$ vector pointing toward vapor phase (positive *z*-direction). This demonstrates that, due to the asymmetry on the molecular plane caused by the methyl group, M-Gdm^+ has a strongly hydrophobic partition that favors the vapor phase. These configurations correspond to the perpendicular configurations shown in Figure 4b, consequently reducing the probability of parallel configurations. We also find that when M-Gdm^+ is near the position z = 15 Å there is a strong enhancement of large $\langle cos\beta\rangle$ (as shown with the white arrow in Figure 4d), which is also confirmed by calculating the $\langle P_2(cos\beta)\rangle$ (shown in Figure 4c). It implies that when the M-Gdm^+ is 3–4 Å below the GDS, the C-$NH(CH_3)$ vector has a strong tendency of pointing to the vapor phase; however, when the cation is right on the GDS, this tendency is somehow weakened. More discussion of this behavior will be continued in the following section.

C. Surface Fluctuation

1. Surface Fluctuation: Relation to Orientation of Guanidinium Ring—Recent studies have demonstrated an interesting connection between liquid-vapor interfacial stability of chemical species (i.e. a free energy minimum state with the solute at the interface) and the extent to which the presence of these molecular species in the vicinity of the interface induces collective fluctuations of the interface in addition to the level inherent in pure water due to thermal motion. In the next discussion, we explore the differences in interfacial fluctuations for the various orientations discussed in the preceding section. We aim to further demonstrate the connection between interfacial stability and fluctuations, and later discuss the implications of this connection for mechanisms of osmolyte influence on macromolecules. We first briefly discuss the protocol to generate a coarse-grained interface from the atomically-discrete representation used via the atomistic force field, and then consider the behavior of fluctuations.

For an instantaneous surface snapshot, the local density profile can be defined as[53]:

$$\langle\rho(\vec{r}_{xy},z)\rangle \equiv \frac{1}{A_\xi}\int d^2\vec{r}'_{xy}\rho(\vec{r}_{xy}-\vec{r}'_{xy},z)=\rho[z-h(\vec{r}_{xy})] \quad (10)$$

which describes the short-distance average of the density over an area $A_\xi \sim \xi^2$ at position $\vec{r_{xy}}$. ξ is an inherent correlation length. Here we define $\delta h(\vec{r_{xy}}) = h(\vec{r_{xy}})-z$ as a surface height function. With this definition, $\langle\delta h(\vec{r_{xy}})\rangle = 0$.

From individual snapshots/configurations we construct the coarse-grained instantaneous surface defined by Willard and Chandler[25,54]. Gaussian mass distributions are assigned to each water oxygen atom according to:

$$\Phi(\mathbf{r};\xi)=(2\pi\xi^2)^{-d/2}exp(-r^2/2\xi^2) \quad (11)$$

where r is the magnitude of **r**, ξ is taken as 3.0 Å, and d is the dimensionality (3 in this case). At space-time point (**r**, t), we have the coarse-grained density as

$$\bar{\rho}(\mathbf{r},t)=\sum_j \Phi(|\mathbf{r}-\mathbf{r}_i(t)|;\xi) \quad (12)$$

The interface is determined as the (d − 1)-dimensional manifold with constant value c. In practice, we set up a series of spatial grid points (x, y, z) and compute the corresponding coarse-grained densities ρ(x, y, z) by Equation 12. We use a grid spacing in the x and y dimensions of 1.0 Å; for the z dimension the grid resolution is 0.2 Å. The surface is then obtained as the manifold defined by setting ρ(x, y, z) = $\rho_{bulk}/2$. Averaging instantaneous surfaces ($h_t(x, y)$, at time t) yields the mean surface $\langle h(x, y)\rangle$; furthermore, $\langle \delta h(x, y)\rangle = 0$. Subtracting the mean values from the $h_t(x, y)$ gives $\delta h_t(x, y)$ and the height fluctuations $\delta h_t^2(x, y)$. Using this framework to characterize fluctuations, we probe magnitudes of average interfacial fluctuations with ions residing at various positions along the reaction coordinate.

We use the same convention of θ as in SectionIIIB to discuss fluctuations of instantaneous surfaces as they depend on Gdm^+/M-Gdm^+ orientation relative to the interface. Furthermore, for a particular orientation, θ, we will consider the variation of interface fluctuation as a function of the distance, r, away from the center of the guanidinium ring moving in the x − y plane of the average interface generated from instantaneous interfaces. This average fluctuation we call $\delta h_L^2(r,\theta)$ (L for lateral). In the case of pure TIP4P-FQ (in the absence of ions), $\langle \delta h^2\rangle$ for the current system size is 0.96±0.07 $Å^2$. In our study, we have confirmed that the fluctuation for lateral distance far away from the center of the cation (r = 20 Å) is consistent with the value of pure TIP4P-FQ. We therefore define $\delta h_L^2(r,\theta)$ as the conditional fluctuations normalized by 0.96 $Å^2$. In this convention, when $\langle \delta h_L^2\rangle$ equals 1, the effect of cation is zero; when $\langle \delta h_L^2\rangle > 1$, the surface height fluctuation is enhanced relative to pure water with the presence of ion; when $\langle \delta h_L^2\rangle < 1$, the surface height fluctuation is suppressed. Furthermore, when we consider all the orientations at the same value of the reaction coordinate, the overall $\delta h_L^2(r)$ will be the weighted linear combination of different θ conditions

$$\langle \delta h_L^2(r)\rangle=\sum_\theta P(\theta)\cdot\langle \delta h_L^2(r,\theta)\rangle \quad (13)$$

while P(θ) is the probability of θ condition (i.e., the probability of observing a particular value of the angle θ).

The results of $\langle \delta h_L^2(r,\theta)\rangle$ for single Gdm^+/M-Gdm^+ at various positions using parallel and perpendicular conditions are shown in Figure 5a, b, d and e. That the parallel orientation induces the largest interfacial fluctuation enhancement is evident for both cations; the peak

fluctuation is roughly twice that of the inherent pure water thermal fluctuation. At positions of 18 and 20 Å, the fluctuations are suppressed relative to pure water, again for both cations. Panels b and e of Figure 5 show reduction in interfacial enhancement for both ions; the Gdm^+ shows a more dramatic decrease. We attribute this to the fact that M-Gdm^+ is larger, and its hydrophobic methyl group, which is projected towards the GDS, maintains the perturbation of the interface. The behavior here is remarkably similar to that observed for simple mono-valent anions that display differential interfacial stabilities at the aqueous liquid-vapor interface. In the case of larger, less charge-dense anions that exhibit non-trivial free energy minima in their PMF's, interfacial fluctuations are significantly enhanced over the pure water case. In the present situation, for the Gdm^+ cation, again, a fairly low charge-density molecular ion, we observe a correlation with surface stability and enhanced interfacial perturbation, but in this case with the conditional requirement that the molecular solute present a particular orientation relative to the interfacial plane. The importance of this orientation in terms of hydration will be addressed further below. The probability weighted $\delta h_{\mathrm{L}}^2(r)$ for single Gdm^+/M-Gdm^+ is shown in Figure 5c and f. As expected, combining the fluctuations from all the possible orientations gives rise to overall fluctuation profiles that are intermediate between the zero and 90 degree orientations. We next consider the variation of the $\delta h_{\mathrm{L}}^2(r{=}0,\theta)$ with the position of the cation along the interface normal reaction coordinate (for a series of four orientation angles, the value of $\delta h_{\mathrm{L}}^2(r,\theta)$ when r = 0 is plotted for points along z). These are shown in Figure 6. For clarity, a vertical offset of 0.25 is added between the curves. In general, independent of species or orientation, $\langle \delta h_{\mathrm{L}}^2 \rangle$ is around 1 when the cation is in the bulk (z = 0 Å). $\langle \delta h_{\mathrm{L}}^2 \rangle$ starts to increase when the cation position is 8 Å below the GDS, reaches to maximum at the position 3.5 Å below the GDS, eventually falls back and shows suppression when the cation is right at the GDS. The maximum fluctuations are accommodated by the smaller angles, with the perpendicular orientations (showing no interface stability) essentially inducing little to no interfacial enhancement. That the parallel orientation induces larger fluctuations coincides with the observation that solvation on this face of the guanidinium ring is weaker than around the periphery of the ring where strong water-cation hydrogen bonding is sustained. Moreover, this behavior is similar with our previous study of surface fluctuations induced by single, low charge density anions[25], and we attempt to explain the current observations by considering the interaction of the local hydration environment of the cation with the solvent and solvent fluctuations at the L-V interface. We aim to show that the two orientations present distinct hydration shell environments towards the interface; the parallel orientation presenting a solvent environment that is less rigid, more malleable, and thus more amenable to inducing fluctuations of the interface as a consequence of a greater disruption of solvent structure on approach to the interface. The perpendicular orientation presents a more rigid hydration environment due to the more effective hydrogen bonding of water in the plane of the ring, thus decreasing the efficacy of this orientation for promoting interfacial fluctuations. These properties of the two orientations are discussed using radial density profiles of water around the single cations and water velocity autocorrelation functions in the hydration shells presented to the interface in the vicinity of the GDS.

We first consider water radial density functions. Previously[25], we demonstrated that spherical, mono-valent anions with PMF minima at the liquid-vapor interfacial region tend to have solvation shells that are in a way fluid (or "malleable"); these solvation shells couple with solvent at the liquid-vapor interface as the anion approaches the interface in a manner that leads to enhancement of the inherent fluctuations of the interface. In contrast to such anions, those species that showed no interfacial stability (PMF minimum) possessed well-ordered, more "rigid" solvation shells that, through little to no coupling with distal solvent on approach to the interface, did not mediate enhanced fluctuations. Thus, ions with interfacial stability possessed complementary solvation shells, while those not stable at the interface did not. Here, we consider the solvation shell environment presented towards the interfacial region as cations of different orientations approach the GDS. In like manner, Gdm^+/M-Gdm^+ induce distinct perturbations of the L-V interface depending on orientation relative to the interface. Figure 7 shows the conditional density of water oxygen $(\rho(r,z), r=\sqrt{x^2+y^2})$ around Gdm^+ for parallel (panel a–c) and perpendicular (panel d–f) configurations at *z*-position = 0, 15, 18 Å, which correspond to the cation in the bulk, the position that induces the largest fluctuation relative to pure water, and a surface state. When Gdm^+ is in the bulk (Figure 7a and d) both configurations shows a bright "ring", corresponding to the first peak of RDF, followed by an outer, darker region signifying the first minimum of RDF. The radius of this "ring" is roughly 3.5 Å. When Gdm^+ is restrained at z = 15 Å, which is roughly 3.5Å below the GDS, the first hydration shell of the parallel configuration merges with the L-V interfacial layer (indicated by white arrows in Figure 7b), while that of perpendicular configuration does not (Figure 7e). For the parallel configuration, the more malleable hydration water above the Gdm^+ plane couples with interfacial water resulting in greater deformation, and resulting fluctuations, of the interface[25] than the perpendicular configuration.

To answer whether hydration water above the plane of the guanidinium ring is less ordered (structured) and diffuse, we analyzed oxygen atom velocity decorrelation functions for water in the region above the guanidinium ring when the cations are in the parallel and perpendicular orientation (relative to the interface) at a z position of 15Å(Figure 8). Oxygen VACF's are computed using well-known expressions[55–57]

$$C_v(t)=\frac{\langle \vec{v}_i(t)\cdot\vec{v}_i(0)\rangle}{\langle \vec{v}_i(0)\cdot\vec{v}_i(0)\rangle} \quad (14)$$

where $\vec{v_i}(t)$ is the velocity vector of the atom (the oxygen in our case) in i_{th} water molecule in the simulation system at time *t*. The brackets denote the ensemble average. Here we only look at the water above the cation and within 5 Å of any atom on the cation. In the Supporting Information (Figure 12) we show that our analysis is independent of whether we use water center of mass or the oxygen atom; thus we discuss water dynamics in terms of the oxygen atom VACF in the main text.

Our analysis shows the similarity of water dynamics above the planar (parallel) orientation to be much like that of the liquid-vapor interface, while that of the perpendicular orientation remains more bulk-like. For the perpendicular orientation when the cation is at z=15Å, we

observe the typical oscillatory behavior signifying a caging effect of local hydrating water molecules on a central solvent molecule. At the bulk position, z=0Å, hydration waters are bulk like for both orientations. This difference was also observed for monovalent halide anions exhibiting contrasting surface stabilities.

2. Surface Fluctuation: Relation to Orientation of Methyl Group of M-Gdm$^+$— We next address behavior of the angle β when M-Gdm$^+$ resides in the L-V interface region (as shown in Figure 4d). Recall we define the angle β between the positive *z*-axis and the vector constructed from center carbon to the nitrogen of -NH(CH_3) ($\overrightarrow{CN_M}$) for M-Gdm$^+$. We use the idea of conditional surface fluctuation to explain this preference with M-Gdm$^+$'s structure. Again we can define

$$\langle \delta h_L^2(r) \rangle = \sum_{\beta} P(\beta) \cdot \langle \delta h_L^2(r,\beta) \rangle \quad (15)$$

and decompose the surface fluctuation contribution from each β angle at the specific cation restrained position marked in Figure 4d. In practice, we set each angular bin between $\beta_i - \Delta\beta$ and $\beta_i + \Delta\beta$, with $\Delta\beta = 10°$, and β_i = 10, 30, 50, 70, 90, 110, 130, 150, 170°. For β = 0°, $\overrightarrow{CN_M}$ points toward vapor phase (methyl group directed to vapor); for β = 90°, $\overrightarrow{CN_M}$ is along the *xy*-plane; for β = 180°, $\overrightarrow{CN_M}$ points toward the water bulk (methyl group directed more towards bulk region). The results for β-conditional, normalized fluctuation $\langle \delta h_L^2 \rangle$ for *z* = 14, 15, 16 and 18 Å are presented in Figure 9. Since no sampling for angles larger than 100° was observed, only the angles less than 100° are considered. For clarity, a vertical offset of 0.1, −0.1 and −0.1 is added for *z* = 14, 15 and 18 Å (Figure 9a, b and d), respectively. At the window of largest probability-weighted fluctuation (*z* = 14 Å, shown in Figure 5f), we notice that $\langle \delta h_L^2 \rangle$ decreases as $\overrightarrow{CN_M}$ points from vapor phase to the *xy*-plane; however, at the following window (*z* = 15 Å) although all the orientations still show enhanced fluctuations, this trend of β-dependence is reversed (also shown in the inset of panel b). At the next following window, *z* = 16 Å, we even found that as $\overrightarrow{CN_M}$ points more toward vapor phase, the M-Gdm$^+$ starts to suppress the interfacial fluctuations. As the M-Gdm$^+$ moves to the GDS (*z* = 18 Å), all β-orientations show similar magnitude of fluctuation suppression. Based on the previous discussion connecting θ-conditional surface stability and interfacial fluctuation, it is natural to consider this β-preference as another manifestation of the drive to maximize fluctuation; this also leads to maximizing interfacial entropy as the two are related through spatial correlations of fluctuations[26]. At *z* = 14 Å, $\overrightarrow{CN_M}$ points towards the vapor, facilitating the largest fluctuations; thus, small β angles are preferred. As M-Gdm$^+$ approaches the GDS, $\overrightarrow{CN_M}$ residing in the *xy*-plane leads to larger fluctuations, consequently the preference of β shifts to larger angles (as demonstrated with the white arrow in Figure 4d). As M-Gdm$^+$ approaches a critical position, $\overrightarrow{CN_M}$ pointing toward vapor phase causes the suppression of interfacial fluctuation, which forces the cation to show higher probability of large β, as evidenced in the $\langle P_2(cos\beta) \rangle$ in Figure 4c. Structurally, it indicates that the methyl group prefers to be partially desolvated rather than fully desolvated. We note that for

the β-dependence analysis presented here, we are actually considering the average over all possible θ values. Although not pursued here, it would be interesting to study δh_{L}^2 as a function of both θ and β.

IV. SUMMARY AND CONCLUSIONS

Via all-atom molecular dynamics simulations, we have shown that though on average there is no liquid-vapor interfacial propensity for either the Gdm^+ or M-Gdm^+ cations, there is a stark orientation-based dispersion of stabilities. Orientations of the guanidinium ring parallel to the interfacial plane are unambiguously more stable (though we do not make any strong claims on the relative stability with the force field based analysis here). Our results recapitulate the differential stabilities observed for the parallel and perpendicular orientations observed in Reference[43]. Furthermore, we find that the configurations that show a PMF minimum at the interface also induce strong perturbing interfacial fluctuations defined as the variance from a mean, coarse-grained interface. Orientations of the guanidinium ring parallel to our proxy for a hydrophobic interface are slightly favored over perpendicular ones. The hydration shell environment exposed to the interface on approach of the cation to the interface is intimately coupled to the different fluctuation behaviors observed for the parallel and perpendicular orientations. The parallel orientation presents a solvent environment that is less rigid, more malleable, and thus more amenable to inducing fluctuations of the interface as a consequence of a greater disruption of solvent structure on approach to the interface. The perpendicular orientation presents a more rigid hydration environment due to the more effective hydrogen bonding of water in the plane of the ring, thus decreasing the efficacy of this orientation for promoting interfacial fluctuations. These differential behaviors are consistent with the fact that in bulk solution, the contact ion pair of Gdm^+ shows a distinct preference for pairs that are stacked parallel to one another (rather than perpendicular to one another) as shown in Figure 11 of the Supporting Information. For the force field used, this suggests the ease with which the hydration waters above the guanidinium ring plane are removed to accommodate a second hydrophobic partner. When considering the denaturant properties of guanidinium, and a direct contact mechanism, the results we present here seem to indicate that association with sidechains groups that are not robustly hydrated is a plausible mechanism of action of this osmolyte.

Supplementary Material

Refer to Web version on PubMed Central for supplementary material.

Acknowledgments

The authors acknowledge support from the National Science Foundation (CAREER:MCB:1149802). Computational resources are acknowledged via support from National Institutes of Health (COBRE:P20-RR015588) in the Chemical Engineering Department at the University of Delaware and (COBRE: 5P20RR017716-07) at the University of Delaware, Department of Chemistry and Biochemistry. SP thanks N. Patel for fruitful discussion and encouragement for the duration of this work.

References

1. Enami S, Mishra H, Hoffmann MR, Colussi AJ. Hofmeister Effects in Micromolar Electrolyte Solutions. J. Chem. Phys. 2012; 136:154707, 1–5. [PubMed: 22519343]
2. Jungwirth P, Tobias DJ. Specific ion effects at the air/water interface. Chem. Rev. 2006; 106:1259–1281. [PubMed: 16608180]
3. Jungwirth P, Tobias DJ. Molecular Structure of Salt Solutions: A New View of the Interface with Implications for Heterogeneous Atmospheric Chemistry. J. Phys. Chem. B. 2001; 105:10468–10472.
4. Petersen PB, Saykally RJ. Confirmation of Enhanced Anion Concentration at the Liquid Water Surface. Chem. Phys. Lett. 2004; 397:51–55.
5. Petersen PB, Saykally RJ, Mucha M, Jungwirth P. Enhanced Concentration of Polarizable Anions at the Liquid Water Surface: SHG Spectroscopy and MD Simulations of Sodium Thiocyanide. J. Phys. Chem. B. 2005; 109:10915–10921. [PubMed: 16852329]
6. Petersen PB, Saykally RJ. Probing the Interfacial Structure of Aqueous Electrolytes with Femtosecond Second Harmonic Generation Spectroscopy. J. Phys. Chem. B. 2006; 110:14060–14073. [PubMed: 16854101]
7. Robertson WH, Johnson MA. Molecular Aspects of Halide Ion Hydration: The Cluster Approach. Annu. Rev. Phys. Chem. 2003; 54:173–213. [PubMed: 12626732]
8. Petersen PB, Saykally RJ. On the Nature of Ions at the Liquid Water Surface. Annu. Rev. Phys. Chem. 2006; 57:333–364. [PubMed: 16599814]
9. Walker DS, Richmond GL. Depth Profiling of Water Molecules at the Liquid-Liquid Interface Using a Combined Surface Vibrational Spectroscopy and Molecular Dynamics Approach. J. Am. Chem. Soc. 2007; 129:9446–9451. [PubMed: 17616192]
10. Walker DS, Richmond GL. Understanding the Effects of Hydrogen Bonding at the Vapor-Water Interface: Vibrational Sum Frequency Spectroscopy of H_2O/HOD/D_2O Mixtures Studied Using Molecular Dynamics Simulations. J. Phys. Chem. C. 2007; 111:8321–8330.
11. Richmond GL. Molecular Bonding and Interactions at Aqueous Surfaces as Probed by Vibrational Sum Frequency Spectroscopy. Chem. Rev. 2002; 102:2693–2724. [PubMed: 12175265]
12. Liu W-T, Zhang L, Shen YR. Interfacial Structures of Methanol: Water Mixtures at a Hydrophobic Interface Probed by Sum-Frequency Vibrational Spectroscopy. J. Chem. Phys. 2006; 125:144711, 1–6. [PubMed: 17042635]
13. Chen Z, Ward R, Tian Y, Baldelli S, Opdahl A, Shen YR, Somorjai GA. Detection of Hydrophobic end Groups on Polymer Surfaces by Sum-Frequeny Generation Vibration Spectroscopy. J. Am. Chem. Soc. 2000; 122:10615–10620.
14. Levin Y. Polarizable Ions at Interfaces. Phys. Rev. Lett. 2009; 102:147803 1–147803 4. [PubMed: 19392484]
15. Levin Y, dos Santos AP, Diehl A. Ions at the Air-Water Interface: an End to a Hundred-Year-Old Mystery? Phys. Rev. Lett. 2009; 103:257802, 1–4. [PubMed: 20366288]
16. Schelero N, von Klitzing R. Correlation between Specific Ion Adsorption at the Air/Water Interface and Long-Range Interactions in Colloidal Systems. Soft Matt. 2011; 7:2936–2942.
17. Parsons DF, Boström M, Nostro PL, Ninham BW. Hofmeister Effects: Interplay of Hydration, Nonelectrostatic Potentials, and Ion Size. Phys. Chem. Chem. Phys. 2011; 13:12352–12367. [PubMed: 21670834]
18. Godec A, Merzel F. Physical Origin Underlying the Entropy Loss upon Hydrophobic Hydration. J. Am. Chem. Soc. 2012; 134:17574–17581. [PubMed: 23003674]
19. Mason PE, Neilson GW, Enderby JE, Saboungi ML, Dempsey CEAD, MacKerell J, Brady JW. The Structure of Aqueous Guanidinum in Chloride Solutions. J. Am. Chem. Soc. 2004; 126:11462–11470. [PubMed: 15366892]
20. Mason PE, Neilson GW, Dempsey CE, Barnes AC, Cruickshank JM. The Hydration Structure of Guanidinium and Thiocyanate Ions: Implications for Protein Stability in Aqueous Solution. Proc. Nat. Aca. Sci. 2003; 100:4557–4561.

21. Rsgen J, Pettitt BM, Bolen DW. An Analysis of the Molecular Origin of Osmolyte-Dependent Protein Stability. Protein Science. 2007; 16:733–743. [PubMed: 17327389]
22. Scott JN, Nucci NV, Vanderkooi JM. Changes in Water Stucture Induced by the Guanidinium Cation and Implications for Protein Denaturation. J. Phys. Chem. A. 2008; 112:10939–10948. [PubMed: 18839935]
23. Kumar A. Aqueous Guanidinium Salts Part II. Isopiestic Osmotic Coefficients of Guanidinium Sulphate and Viscosity and Surface Tension of Guanidinium Chloride, Bromide, Acetate, Perchlorate and Sulphate Solutions at 298.15 K. Fluid Phase Equilibria. 2001; 180:195–204.
24. Koishi, T.; Yasuoka, K.; Willow, SY.; Fujikawa, S.; Zeng, XC. J. Chem. Theory Comput. ASAP; 2013. Molecular Insight into Different Denaturing Efficiency of Urea, Guanidinium, and Methanol: A Comparative Simulation Study.
25. Ou S, Patel S. Temperature Dependence and Energetics of Single Ions at the Aqueous Liquid-Vapor Interface. J. Phys. Chem. B. 2013; 117:6512–6523. [PubMed: 23537166]
26. Otten DE, Shaffer PR, Geissler PL, Saykally RJ. Elucidating the Mechanism of Selective Ion Adsorption to the Liquid Water Surface. Proc. Nat. Aca. Sci. 2012; 109:701–705.
27. Dang LX. Computational Study of Ion Binding to the Liquid Interface of Water. J. Phys. Chem. B. 2002; 106:10388–10394.
28. Dang LX, Chang TM. Molecular Mechanism of Ion Binding to the Liquid/Vapor Interface of Water. J. Phys. Chem. B. 2002; 106:235–238.
29. Wick CD, Dang LX. Recent Advances in Understanding Transfer Ions Across Aqueous Interfaces. Chem. Phys. Lett. 2008; 458:1–5.
30. Brooks BR, Brooks CL III, MacKerell AD Jr, Nilsson L, Petrella RJ, Roux B, Won Y, Archontis G, Bartels C, Boresch S, et al. CHARMM: The Biomolecular Simulation Program. J. Comp. Chem. 2009; 30:1545–1614. [PubMed: 19444816]
31. Nosé S. A Molecular Dynamics Methods for Simulations in the Canonical Ensemble. Mol. Phys. 1984; 52:255–268.
32. Rick SW, Stuart SJ, Berne BJ. Dynamical Fluctuating Charge Force Fields: Application to Liquid Water. J. Chem. Phys. 1994; 101:6141–6156.
33. Darden T, York D, Pedersen L. Particle Mesh Ewald: An $N \cdot \log(N)$ Method for Ewald Sums in Large Systems. J. Chem. Phys. 1993; 98:10089–10092.
34. Essmann U, Darden T, Lee H, Perera L, Berkowitz ML, Pederson L. A Smooth Particle Mesh Ewald Method. J. Chem. Phys. 1995; 103:8577–8593.
35. Allen, MP.; Tildesley, DJ. Computer Simulations of Liquids. Clarendon: 1987.
36. Wong K-Y, York DM. Exact Relation between Potential of Mean Force and Free-Energy Profile. J. Chem. Theory Comput. 2012; 8:3998–4003. [PubMed: 23185141]
37. Kumar S, Bouzida D, Swendsen RH, Kollman PA, Rosenberg JM. The Weighted Histogram Analysis Method for Free-Energy Calculations on Biomolecules. I. The Method. J. Comp. Chem. 1992; 13:1011–1021.
38. Zhu F, Hummer G. Convergence and Error Estimation in Free Energy Calculations Using the Weighted Histogram Analysis Method. J. Comp. Chem. 2012; 33:453–465. [PubMed: 22109354]
39. Flyvbjerg H, Petersen HG. Error Estimates on Averages of Correlated Data. J. Chem. Phys. 1989; 91:461–466.
40. Patel S, Brooks CL III. CHARMM Fluctuating Charge Force Fields for Proteins: I Parameterization and Application to Bulk Organic Liquid Simulations. J. Comp. Chem. 2004; 25:1–15. [PubMed: 14634989]
41. Patel S, MacKerell AD Jr, Brooks CL III. CHARMM Fluctuating Charge Force Fields for Proteins: II- Protein/Solvent Properties from Molecular Dynamics Simulations Using a Nonadditive Electrostatic Model. J. Comp. Chem. 2004; 25:1504–1514. [PubMed: 15224394]
42. Ou S, Lucas TR, Zhong Y, Bauer BA, Hu Y, Patel S. Free Energetics and the Role of Water in the Permeation of Methyl Guanidinium across the Bilayer-Water Interface: Insights from Molecular Dynamics Simulations Using Charge Equilibration Potentials. J. Phys. Chem. B. 2013; 117:3578–3592. [PubMed: 23409975]

43. Wernersson E, Heyda J, Vazdar M, Lund M, Mason PE, Jungwirth P. Orientational Dependence of the Affinity of Guanidinium Ions to the Water Surface. J. Phys. Chem. B. 2011; 115:12521–12526. [PubMed: 21985190]
44. Warren GL, Patel S. Hydration Free Energies of Monovalent Ions in Transferable Intermolecular Potential Four Point Fluctuating Charge Water: An Assessment of Simulation Methodology and Force Field Performance and Transferability. J. Chem. Phys. 2007; 127:064509. [PubMed: 17705614]
45. Warren GL, Patel S. Comparison of the Solvation Structure of Polarizable and Nonpolarizable Ions in Bulk Water and Near the Aqueous Liquid-Vapor Interface. J. Phys. Chem. C. 2008; 112:7455–7467.
46. Warren GL, Patel S. Electrostatic Properties of Aqueous Salt Solution Interfaces: A Comparsion of Polarizable and Nonpolarizable Ion Models. J. Phys. Chem. B. 2008; 112:11679–11693. [PubMed: 18712908]
47. Nosé S. A Unified Formulation of the Constant Temperature Molecular Dynamics Methods. J. Chem. Phys. 1984; 81:511–519.
48. Wick CD, Lee AJ, Rick SW. How Intermolecular Charge Transfer Influences the Air-Water Interface. J. Chem. Phys. 2012; 137:154701. [PubMed: 23083178]
49. Lee AJ, Rick SW. The Effects of Charge Transfer on the Properties of Liquid Water. J. Chem. Phys. 2011; 134:184507. [PubMed: 21568521]
50. Kirkwood JG, Buff FP. The Statistical Mechanical Theory of Surface Tension. J. Chem. Phys. 1949; 17:338–343.
51. D'Auria R, Tobias DJ. Relation between Surface Tension and Ion Absorption at the Air-Water Interface: A Molecular Dynamics Simulation Study. J. Phys. Chem. A. 2009; 113:7286–7293. [PubMed: 19438204]
52. Stern AC, Baer MD, Mundy CJ, Tobias DJ. Thermodynamics of Iodide Adsorption at the Instantaneous Air-Water Interface. J. Chem. Phys. 2013; 138:114709, 1–8. [PubMed: 23534655]
53. Pershan, PS.; Schlossman, M. Liquid Surfaces and Interfaces: Synchrotron X-ray Methods. Cambridge: Cambridge University Press; 2012. p. 4
54. Willard AP, Chandler D. Instantaneous Liquid Interfaces. J. Phys. Chem. B. 2010; 114:1954–1958. [PubMed: 20055377]
55. Rahman A. Correlations in the Motion of Atoms in Liquid Argon. Phys. Rev. 1964; 136:A405–A411.
56. Choudhury N, Pettitt BM. Dynamics of Water Trapped between Hydrophobic Solutes. J. Phys. Chem. B. 2005; 109:6422–6429. [PubMed: 16851715]
57. Marti J, Nagy G, Guardia E, Gordillo MC. Molecular Dynamics Simulation of LiquidWater Confined inside Graphite Channels: Dielectric and Dynamical Properties. J. Phys. Chem. B. 2006; 110:23897–23994.

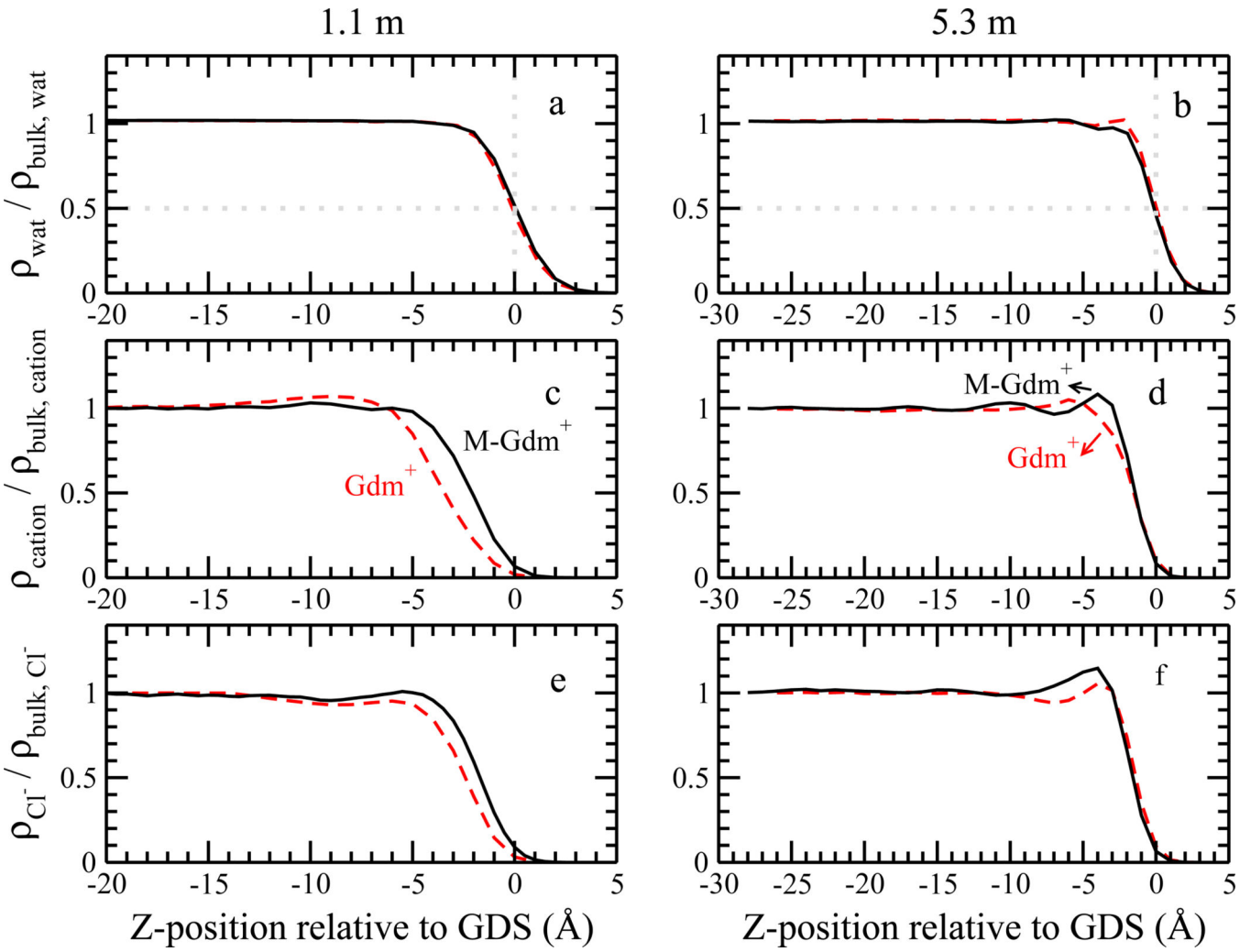

FIG. 1.

Normalized number density profile of water oxygen, solute central carbon atom of ring (Gdm^+ or $M\text{-}Gdm^+$) and Cl^- in 1.1 m and 5.3 m solution.

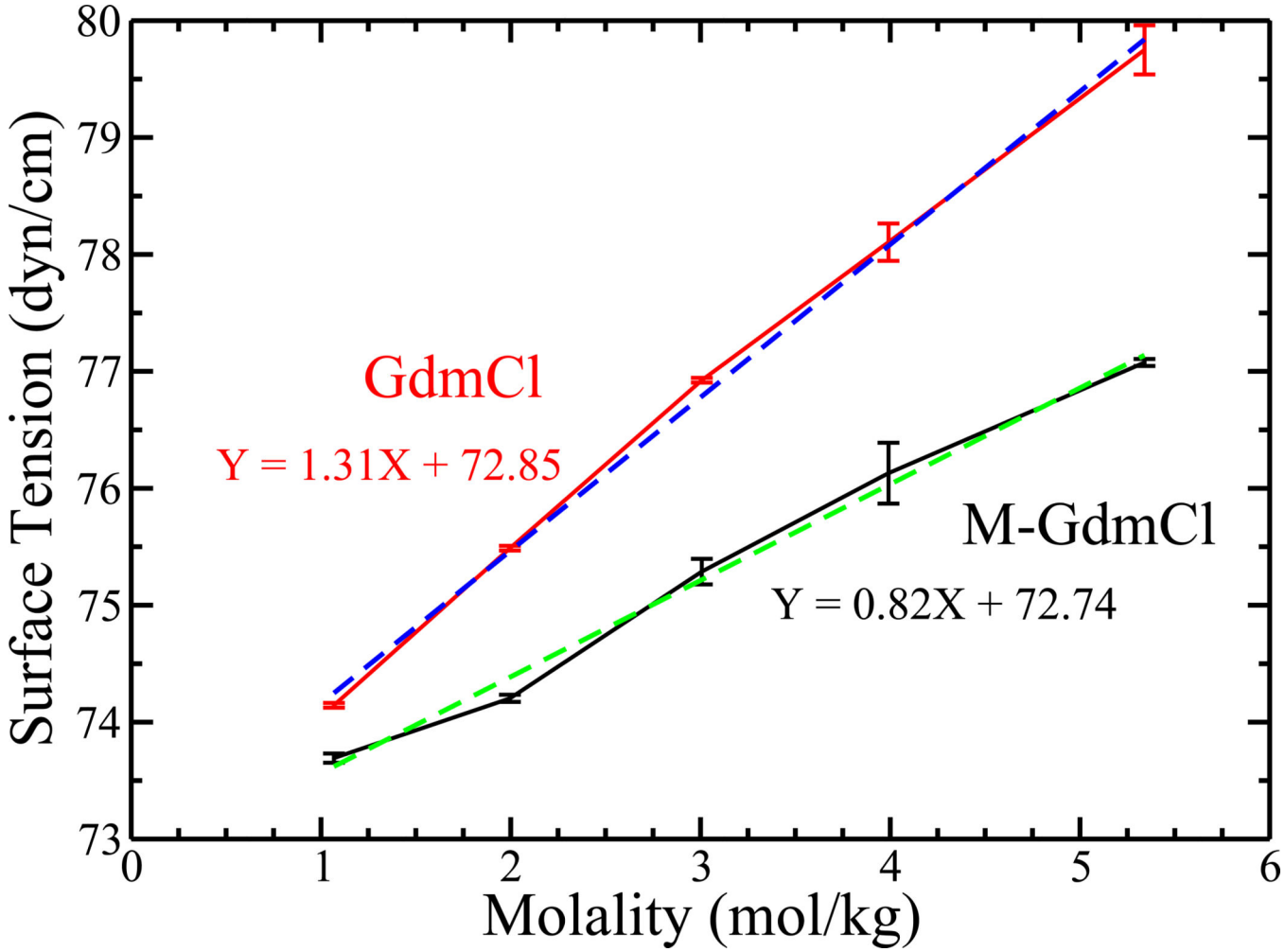

FIG. 2.
Surface tension as a function of concentration, along with the linear fitting results.

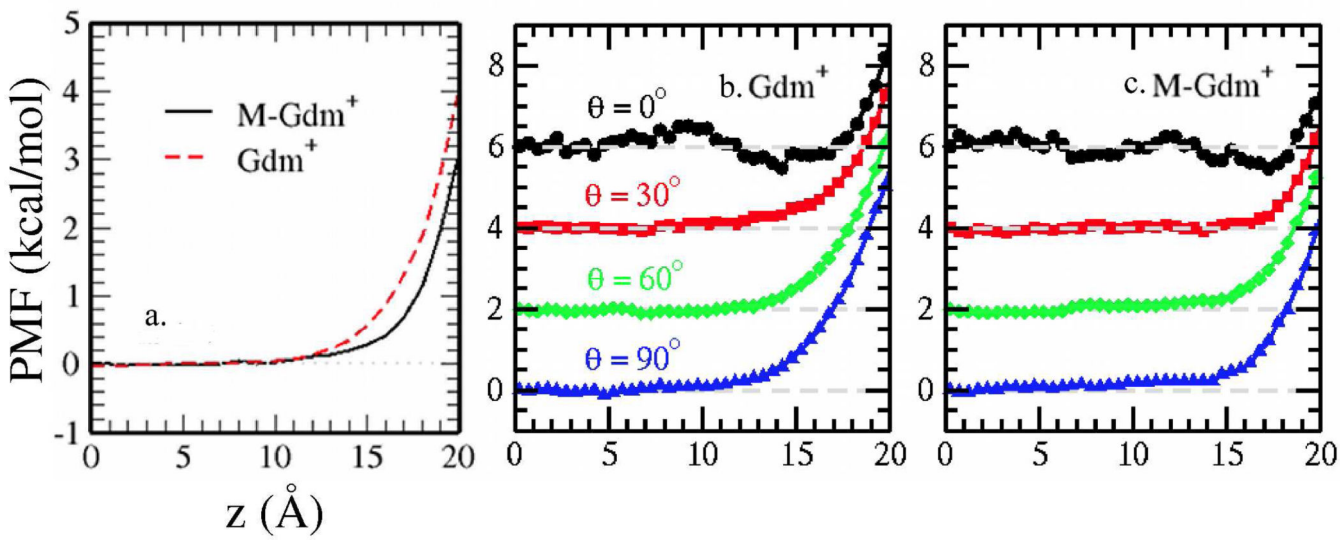

FIG. 3.

(a) Potential of mean force of single Gdm^+/M-Gdm^+ from bulk transporting through L-V interface. Conditional potential of mean force for single (b) Gdm^+ or (c) M-Gdm^+. A vertical offset of 2 kcal/mol is added for clarity.

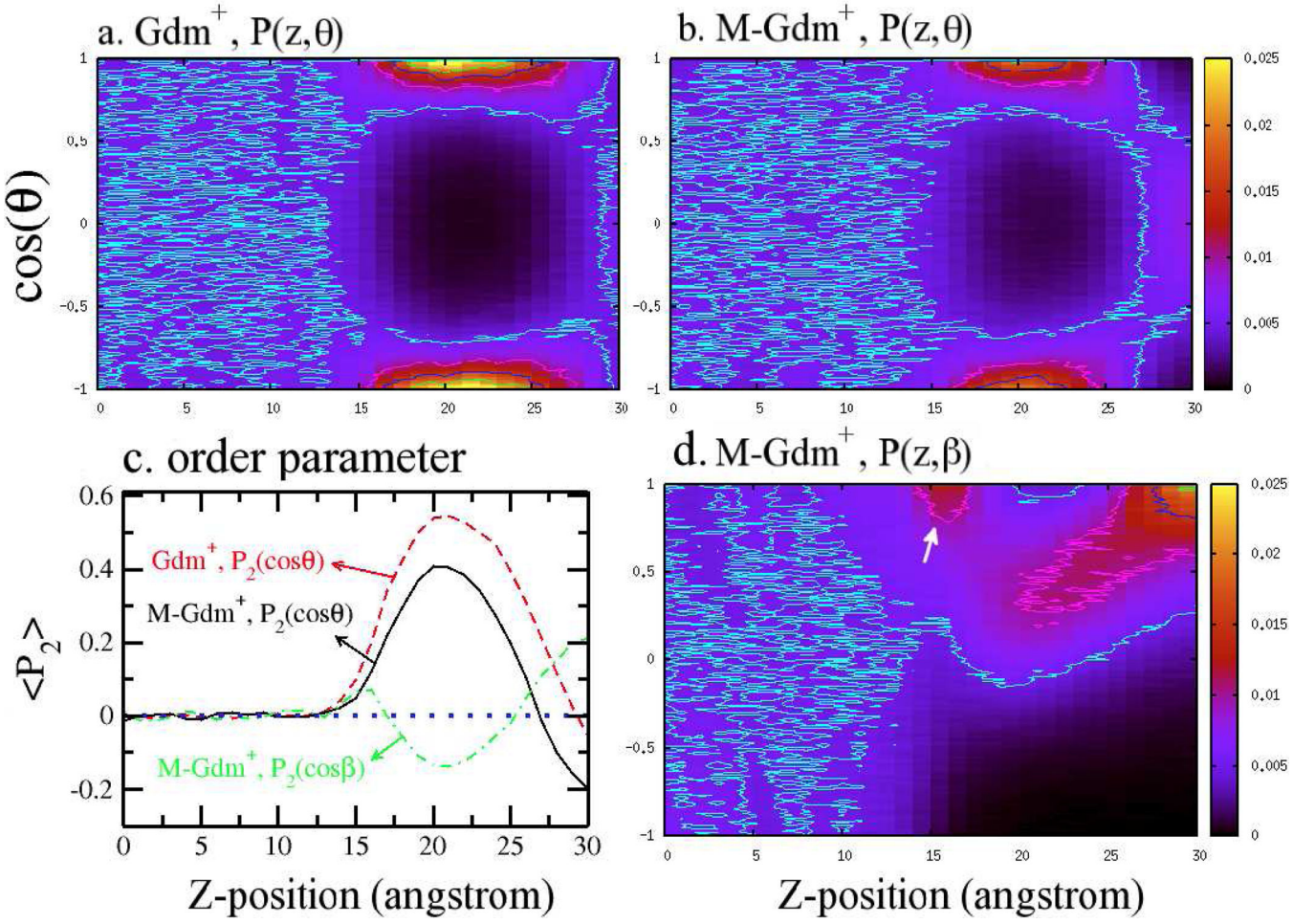

FIG. 4.

Orientational distribution of single Gdm^+ and M-Gdm^+. Refer to text for the definition of θ and β.

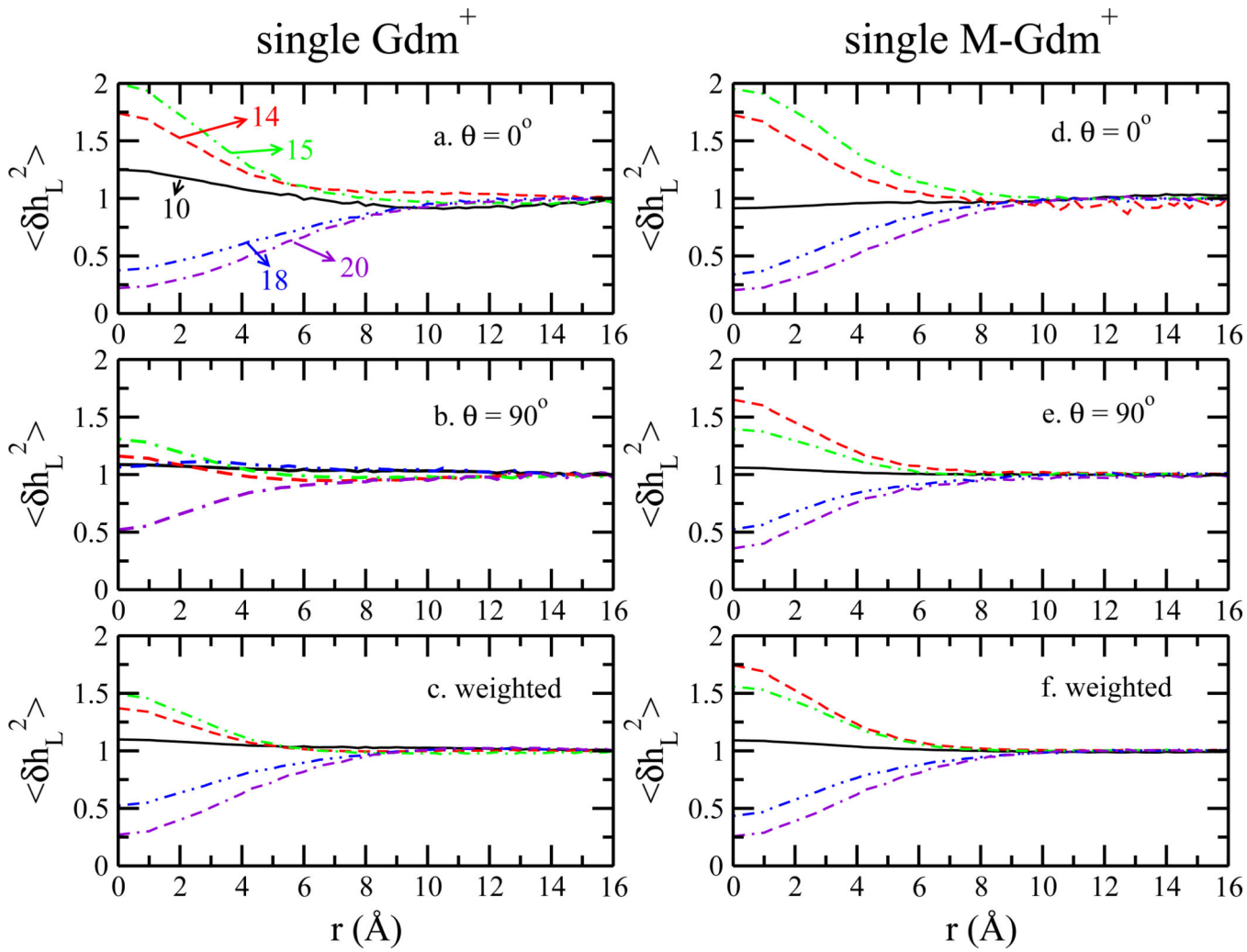

FIG. 5.

Conditional, normalized fluctuation $(\delta h_{\mathrm{L}}^2)$ as a function of *r* from the center carbon of Gdm^+ or M-Gdm^+. (a) Gdm^+, θ = 0 °; (b) Gdm^+, θ = 90 °; (c) Gdm^+, all orientations with probability weighted; (d) M-Gdm^+, θ = 0 °; (e) M-Gdm^+, θ = 90 °; (f) M-Gdm^+, all orientations with probability weighted. The values shown in Panel a (and applicable to all panels) indicate fluctuation profiles for solute positions of 10.0, 14.0, 15.0, 18.0, 20.0 Å from the center of the bulk solution region of the simulation cell.

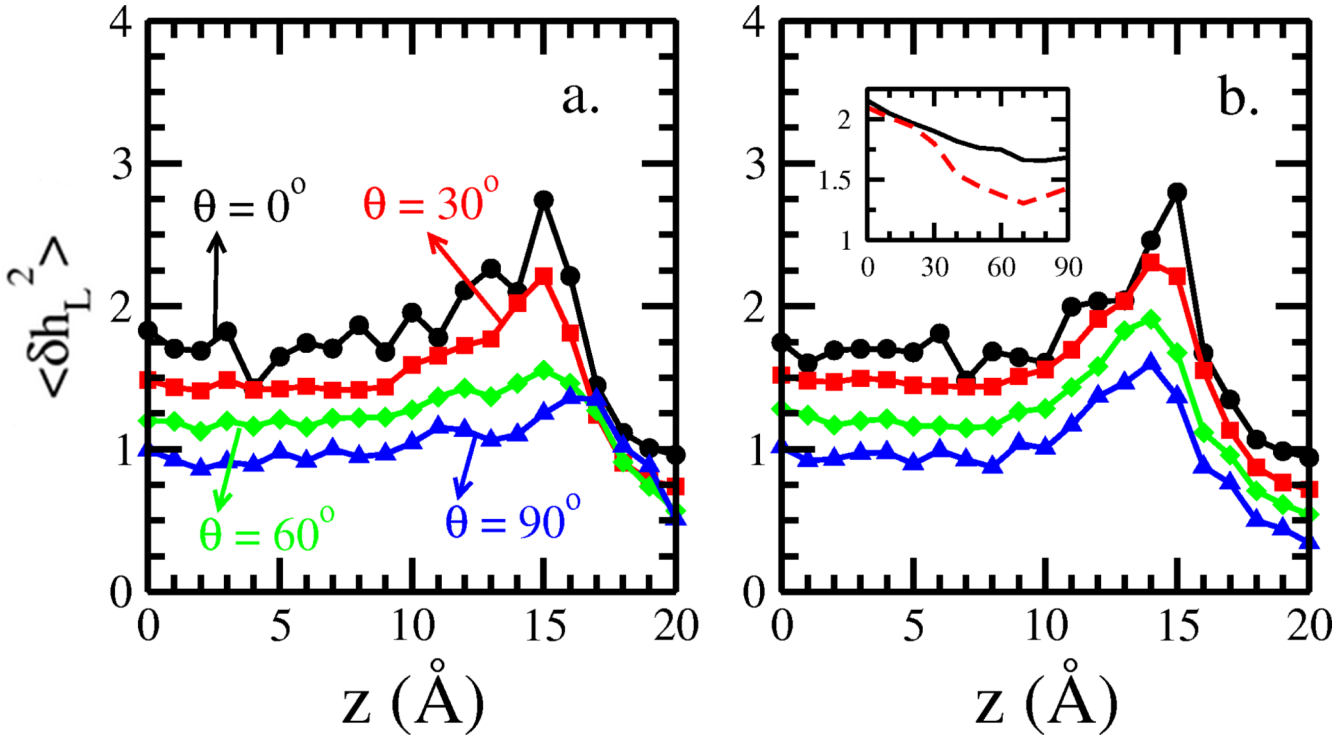

FIG. 6.

The largest, probability weighted, normalized fluctuation (r = 0 Å) as a function of z-position of the (a) Gdm^+ (b) M-Gdm^+. Inset shows the largest conditional fluctuation for each conditional orientation; black solid line is for single M-Gdm^+, while red dashed line corresponds to single Gdm^+.

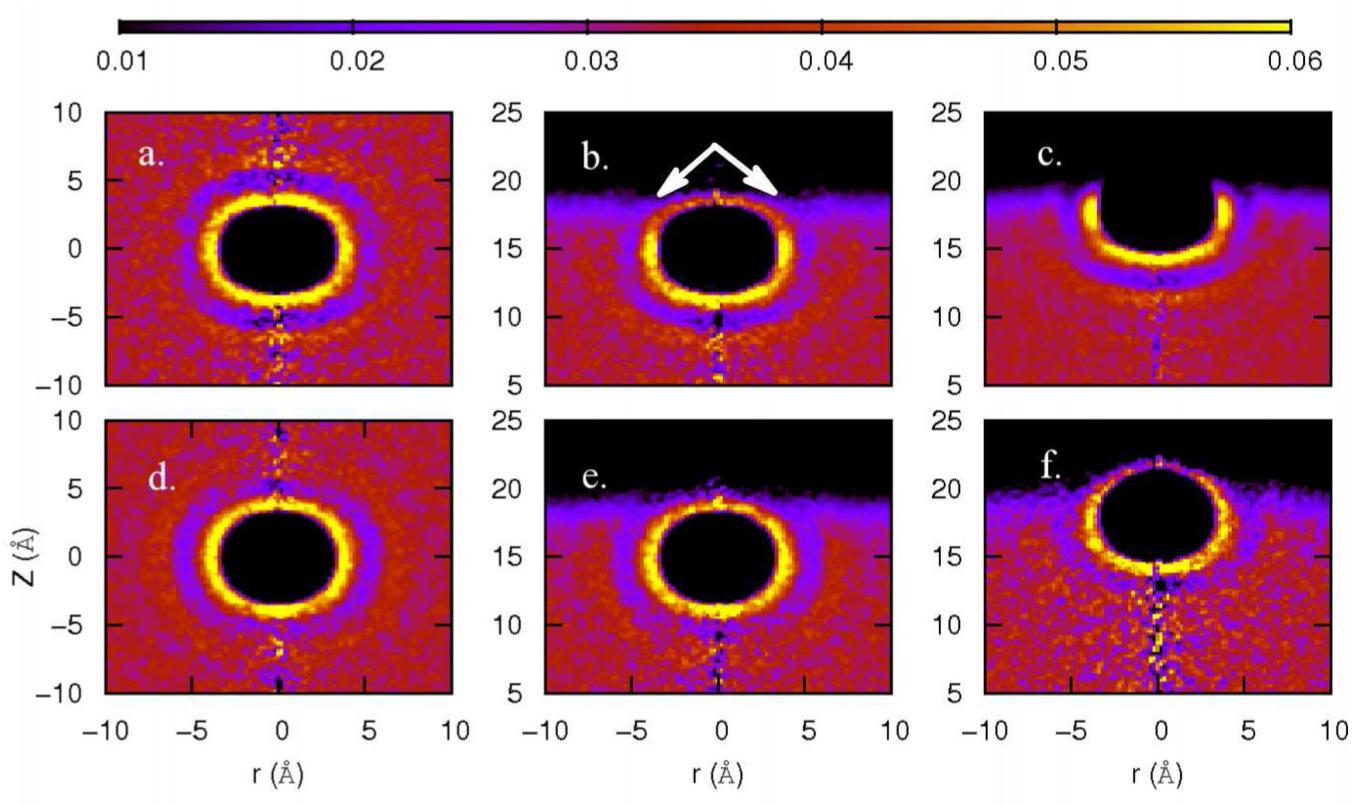

FIG. 7.

Conditional density profiles of single Gdm^+ at different *z*-position. (a) *z* = 0.0 Å, θ = 0 °; (b) *z* = 15.0 Å, θ = 0 °; (c) *z* = 18.0 Å, θ = 0 °; (d) *z* = 0.0 Å, θ = 90 °; (e) *z* = 15.0 Å, θ = 90 °; (f) *z* = 18.0 Å, θ = 90 °.

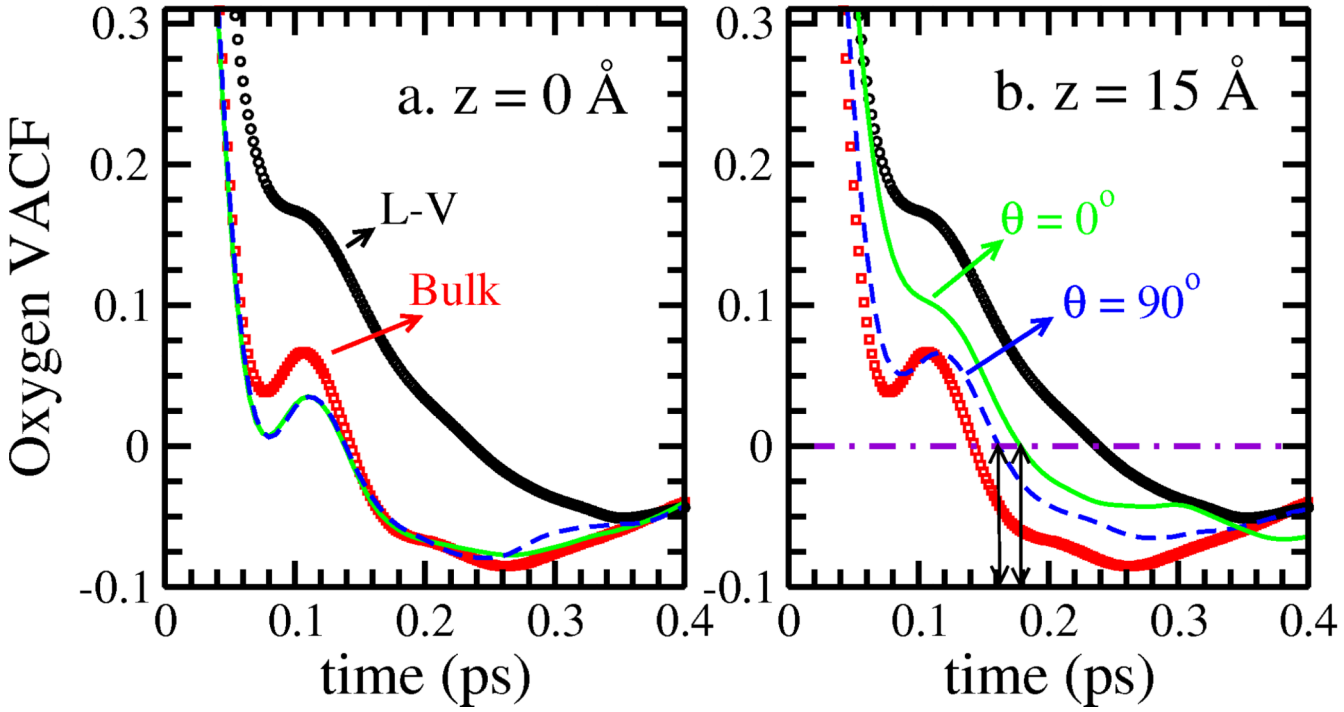

FIG. 8.

Oxygen VACF of water near the Gdm^+ for parallel/perpendicular orientation at (a) bulk (z = 0 Å) and (b) the restrained window with largest fluctuation (z = 15 Å).

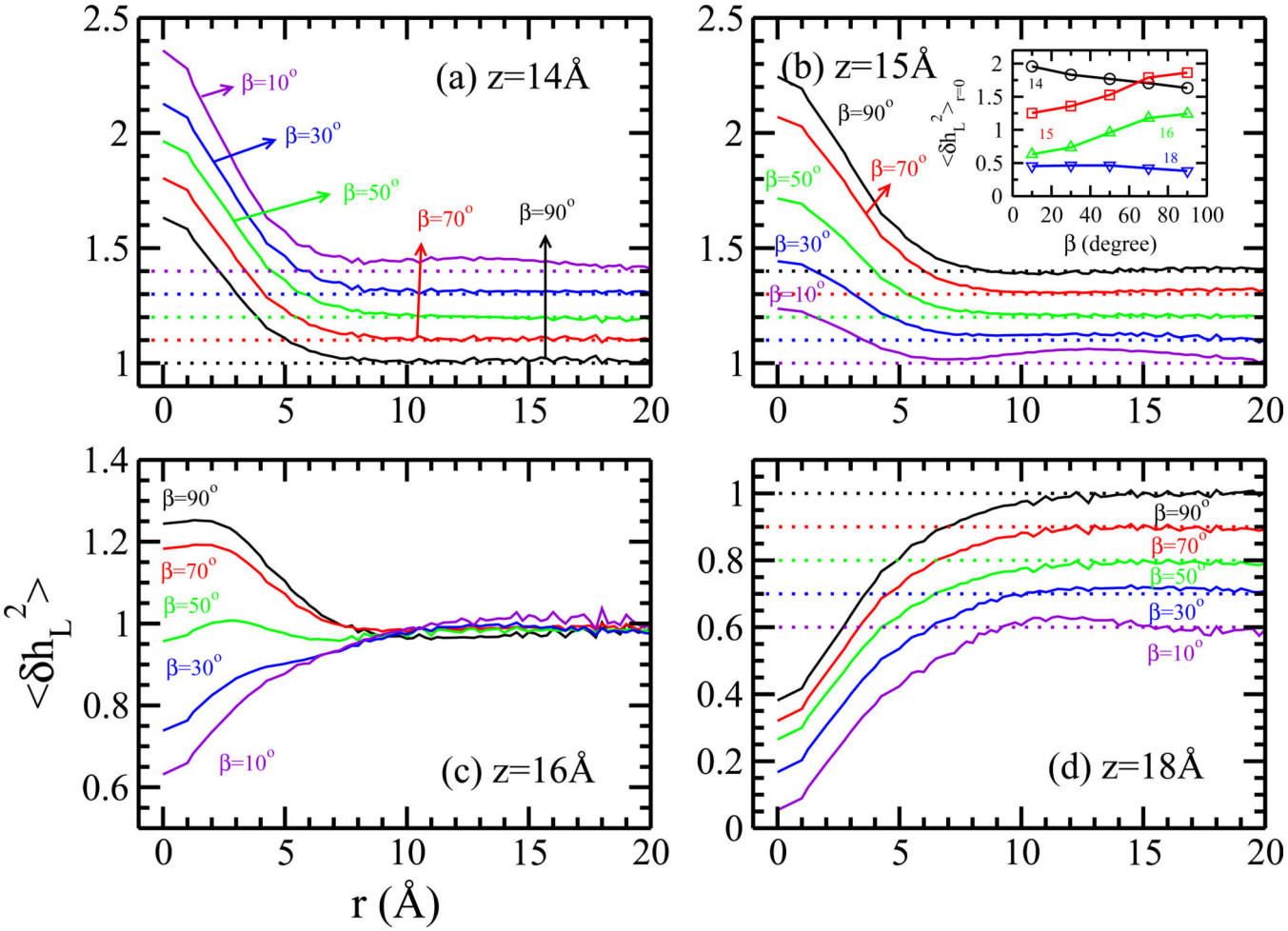

FIG. 9.

β-conditional fluctuation profiles of single M-Gdm$^+$ at different *z*-position. (a) *z* = 14.0 Å (b) *z* = 15.0 Å (c) *z* = 16.0 Å (d) *z* = 18.0 Å. Inset shows the $\langle \delta h_L^2 \rangle$ at *r* = 0 Å from each panel. For clarity, an vertical offset of 0.1, −0.1, −0.1 has been added in window *z* = 14, 15, 18 Å, respectively. In all panels, the y-axis is the normalized fluctuation, $\langle \delta h_L^2 \rangle$ (dimensionless), and the x-axis is radial distance from the solute center of mass.

TABLE I

Properties of the solution systems studied in this manuscript, including the position of Gibbs dividing surface (GDS), mass density (ρ_{mass}) and surface tension (γ). Values in parentheses indicate the uncertainties, which are obtained via the standard deviation of 4 replicates.

System	Pairs of Ions	GDS (Å)	ρ_{mass} (g/cm^3) (calc.)	γ (dyn/cm) (calc.)
GdmCl				
1.1 m	38	20.16	1.015	74.14(0.02)
2 m	71	21.58	1.022	75.49(0.02)
3 m	107	23.13	1.027	76.92(0.02)
4 m	142	24.64	1.032	78.11(0.16)
5.3 m	190	26.68	1.036	79.75(0.21)
M-GdmCl				
1.1 m	38	20.51	1.014	73.69(0.04)
2 m	71	22.23	1.020	74.20(0.03)
3 m	107	24.07	1.025	75.29(0.11)
4 m	142	25.87	1.030	76.13(0.26)
5.3 m	190	28.29	1.035	77.08(0.03)

TABLE II

Surface excess calculated from our simulation and experimental data. $\Gamma^{\pm}_{\mathrm{comp}}$ refers to the surface excess of the cation/anion from our simulation.

System	$\Gamma^{+}_{\mathrm{comp}}$	$\Gamma^{-}_{\mathrm{comp}}$	Γ_{comp}	Γ_{exp}
GdmCl				
1.1 m	−0.017	−0.017	−0.034	−0.022
2 m	−0.031	−0.021	−0.052	−0.031
3 m	−0.033	−0.031	−0.063	
4 m	−0.039	−0.037	−0.077	
5.3 m	−0.039	−0.036	−0.075	
M-GdmCl				
1.1 m	−0.012	−0.014	−0.026	
2 m	−0.017	−0.016	−0.033	
3 m	−0.014	−0.017	−0.031	
4 m	−0.023	−0.022	−0.044	
5.3 m	−0.018	−0.013	−0.031	

TABLE III

Force Field Parameters for Gdm^+, M-Gdm^+ and Cl^-.

Distance[a]	r_0 (Å)	k_B (kcal/mol/Å^2)		
C-N	1.365	463.0		
N-H	1.000	455.0		
N-CT3[b]	1.490	261.0		
Angles[c]	θ_0 (∘)	k_A (kcal/mol/rad^2)		
N-C-N	120.00	52.0		
C-N-H	120.00	49.0		
H-N-H	120.00	25.0		
C-N-CT3	120.00	62.3		
H-N-CT3	120.00	40.4		
N-CT3-HA[d]	107.50	51.5		
HA-CT3-HA	108.40	35.5		
Non-Bonded Parameters[e]	σ (Å)	ε (kcal/mol)	$\frac{1}{2}\eta(\mathrm{kcal/mol/e})$	χ (kcal/mol/e^2)
C	4.450	−0.16000	326.16817	123.33139
N	3.700	−0.20000	350.96041	145.30623
H	1.249	−0.01600	276.49391	297.48634
Cl	4.920	−0.07658	N/A	N/A
CT3	4.040	−0.07300	319.64684	120.17339
HA	2.640	−0.02200	315.55701	250.71405
Dihedrals[f]	k_D (kcal/mol)	n[g]	δ (∘)	
N-C-N-H	2.25	2	180.0	
C-N-CT3-HA	0.00	6	180.0	
Improper Dihedrals[h]	k_I (kcal/mol/*rad*^{2})	ψ		
N-N-N-C	40.0000	0.0000		

[a] $U_B = k_B(r - r_0)^2$.

[b] CT3 is the carbon atom in methyl group.

[c] $U_A = k_A(\theta - \theta_0)^2$.

[d] HA is the hydrogen atom in methyl group.

[e] Lennard-Jones form; geometric combination rules.

[f] $U_D = k_D(1 + cos(n(\chi) - \delta))$.

[g] Multiplicity of the dihedral angles.

[h] $U_I = k_I(\psi - \psi_0)^2$.